Sagnac interferometry with a single atomic clock

R. Stevenson,[1] M.R. Hush,[1,2] T. Bishop,[1] I. Lesanovsky,[1] and T. Fernholz[1,*]

[1] *School of Physics & Astronomy, University of Nottingham, Nottingham NG7 2RD, United Kingdom*
[2] *School of Engineering and Information Technology, University of New South Wales at the Australian Defence Force Academy, Canberra 2600, Australia*

(Dated: October 21, 2015)

The Sagnac effect enables interferometric measurements of rotation with high precision. Using matter waves instead of light promises resolution enhancement by orders of magnitude that scales with particle mass. So far, the paradigm for matter wave Sagnac interferometry relies on DeBroglie waves and thus on free propagation of atoms either in free fall or within waveguides. However, the Sagnac effect can be expressed as a propertime difference experienced by two observers moving in opposite directions along closed paths and has indeed been measured with atomic clocks flown around Earth. Inspired by this, we investigate an interferometer comprised of a single atomic clock. The Sagnac effect manifests as a phase shift between trapped atoms in different internal states after transportation along closed paths in opposite directions, without any free propagation. With analytic models, we quantify limitations of the scheme arising from atomic dynamics and finite temperature. Furthermore, we suggest an implementation with previously demonstrated technology.

PACS numbers: 37.25.+k, 03.75.Dg, 42.81.Pa, 03.75.-b

The most sensitive Sagnac interferometers to date are large ring lasers [1]. The large Wettzell laser gyroscope, e.g., achieves a theoretical resolution of $10^{-11}\mathrm{rad}/\sqrt{\mathrm{s}}$ [2]. The potentially enormous gain in sensitivity when using massive particles [3] has attracted considerable efforts to build matter wave interferometers [4]. Despite the immense challenges in achieving similar particle flux and interferometer areas as with photons, atomic gyroscopes [5, 6] have reached performance levels that should enable applications in fundamental physics, geodesy, seismology, or inertial navigation. Atom interferometers [7] have been demonstrated with record sensitivities below $10^{-9}\mathrm{rad}/\sqrt{\mathrm{s}}$ [8, 9] outperforming commercial navigation sensors by orders of magnitude. Recent experiments aim at geodetic [10] and navigational applications combining multi-axis measurements of acceleration and rotation [11, 12]. Since free falling atoms require large apparatus size, ring shaped traps and guided interferometers have been proposed [13–16] and implemented [17–22] for a variety of geometries and levels of sophistication [23–25]. But guided interferometers with high sensitivity have yet to be demonstrated.

So far, all demonstrated and suggested schemes employ free propagation of particles along the interfering paths. However, measurement of the Sagnac effect does not require free propagation of matter waves. In fact, it has been measured by comparing atomic clocks flown around Earth [28]. Here, we show that the effect can be observed with a single atomic clock. The scheme uses the acquired phase shift between atoms in two different internal clock (spin) states that are each fully confined in atom traps but separately displaced. This approach, for which we suggest a specific implementation following ref. [30], offers a high degree of control over atomic motion. It removes velocity dependent effects and, most importantly, interferometric stability requirements on optical control fields and interferometer paths. It improves control of heating from waveguide corrugations and avoids wave packet dispersion allowing for multiple revolutions.

The situation for fully confined atoms can be depicted in an inertial frame, as seen in Fig. 1. Two independent traps, each containing atoms of rest mass m are displaced around a ring of radius r. Starting from a common angular position at $\theta = 0$, the traps are moved along counter-propagating trajectories and recombined at multiples of the half-revolution time T. From the experimenter's point of view, who defines the trajectories, this happens on the opposite side of the ring and at the original starting point. But if the laboratory frame is rotating at angular frequency ω_S, the first recombination will occur at $\theta = \pi + \omega_\mathrm{S} T$. In the inertial frame, the traps will therefore be displaced at different average angular speeds $\omega_\pm = \pi/T \pm \omega_\mathrm{S}$, leading to a propertime difference of $\Delta\tau_\mathrm{p} \approx 2\pi\omega_\mathrm{S} r^2/c^2$ for the two co-moving rest frames, proportional to interferometer area. In these co-moving frames each atomic state can be described as evolving at its respective Compton frequency $\omega_C = mc^2/\hbar$ [26, 27], leading to a phase difference $\Delta(\omega_\mathrm{C}\tau_\mathrm{p}) \approx \omega_\mathrm{C}\Delta\tau_\mathrm{p} + \Delta\omega_\mathrm{C}\tau_\mathrm{p}$ for non-relativistic speeds and energies (apart from evolution due to the confining potentials, which we endeavour to make the same in both paths). The first term, which is equivalent to the propagation phase difference in the inertial frame, leads to the Sagnac phase for a half revolution $\phi_\mathrm{S} \approx 2\pi\omega_\mathrm{S} r^2 m/\hbar$, which advances any dynamical phase $\Delta\omega_\mathrm{C}\tau_\mathrm{p} \approx \Delta E T/\hbar$ resulting from energy differences ΔE that can be included in the rest mass, e.g., different internal energies of two clock states. This argument shows that the Sagnac phase can indeed be measured accurately in a fully guided setting, as long as the internal energy difference is precisely known or compensated, and shifts

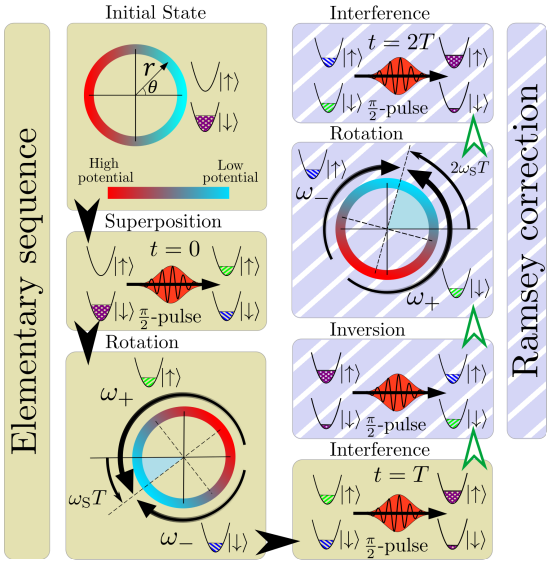

Figure 1. Experimental sequence. The situation is depicted in an inertial frame. Starting with atoms prepared in $|\downarrow\rangle$ located at $\theta = 0$, a $\pi/2$-pulse generates a superposition of two non-degenerate internal states. Atoms in $|(\uparrow)\downarrow\rangle$ are then transported along a circular path in (anti-)clockwise direction. After a half-revolution, a second pulse converts any phase shift into population difference, which is measured in the elementary sequence (black arrows). An extended Ramsey sequence (green arrows) can be used to achieve full common path operation. Here, the $\pi/2$-pulse at time T is extended to a π-pulse, fully inverting the atomic states. Transport is continued such that all atoms complete a full revolution before converting and measuring the phase difference at time $2T$.

due to confinement or external effects remain identical when observed in the two rest frames.

Interferometer sequence. Our scheme requires state-dependently controlled trapping potentials moved around a ring in combination with a Ramsey sequence used for atomic clocks, as shown in Fig. 1. In the elementary sequence we study here, each atom is initially trapped at $\theta = 0$ and prepared in a superposition of two non-degenerate spin states $|\Psi\rangle = \frac{1}{\sqrt{2}}(|\downarrow\rangle + |\uparrow\rangle)$ by starting in $|\downarrow\rangle$ and driving a resonant $\pi/2$-pulse derived from a stable reference clock. The state-dependency is then used to move atoms in state $|(\uparrow)\downarrow\rangle$ (anti-)clockwise around the ring. When the two components recombine on the opposite side, they will have acquired a relative phase difference, which is measured by driving a second $\pi/2$-pulse with an adjustable phase $\phi_{\rm ref}$, converting the phase difference into population difference.

In order to remove constant perturbations of the two spin state energies or, equivalently, a constant detuning of the reference clock, a spin echo sequence can be used. The $\pi/2$-pulse at time T is extended to a π-pulse, exchanging states $|\downarrow\rangle$ and $|\uparrow\rangle$, before rotating the state dependent traps in the opposite direction such that each component completes a full revolution over time $2T$. As before, a final $\pi/2$-pulse converts phase difference into measurable number difference. This sequence removes the time-dependent dynamical phase, because all atoms spend half the observer's time in each spin state. While this prevents operation as an atomic clock, it does, however, not remove the path dependent Sagnac phase. This procedure also cancels effects from constant but spatially dependent energy shifts as all atoms travel the same paths in the same spin states. Due to the common path for a full revolution, dynamical phases caused by constant external acceleration, gravitation or other static potentials do not affect the measurement.

Guided interferometer models. In the following, we analyze the effects of fully confined transport and determine conditions that allow for reliable measurements of the Sagnac phase. We neglect any interactions or mixing of the two spin states and describe the dynamics of the interferometer by a Hamiltonian of the form $\hat{H} = \hbar\omega[\hat{H}_\uparrow|\uparrow\rangle\langle\uparrow| + \hat{H}_\downarrow|\downarrow\rangle\langle\downarrow|]$. The frequency scale ω will be specified below. We assume identical shapes for the two state-dependent potentials and equal and opposite paths in the laboratory frame. For the elementary sequence shown in Fig. 1 and atoms starting in motional ground state $|g\rangle$, the final atomic state can be expressed using unitary evolution operators $|\Psi(T)\rangle = \hat{P}(\phi_{\rm ref})\hat{U}(T)\hat{P}(0)|g\rangle\otimes|\downarrow\rangle$, where $\hat{U}(T) = \hat{U}_\uparrow(T)\otimes\hat{U}_\downarrow(T)$ is the evolution imposed by the Hamiltonian and $\hat{P}(\phi)$ describes a $\pi/2$-pulse with phase ϕ. The measured signal is the population difference $\langle\hat{\sigma}_{\rm z}\rangle$, where $\hat{\sigma}_{\rm z} = |\downarrow\rangle\langle\downarrow| - |\uparrow\rangle\langle\uparrow|$. This expression simplifies to

$$\langle\hat{\sigma}_z\rangle = \frac{1}{2}\langle g|\hat{U}_\downarrow^\dagger(T)\hat{U}_\uparrow(T)|g\rangle e^{i\phi_{\rm ref}} + \text{H.c.}, \qquad (1)$$

Control of $\phi_{\rm ref}$ enables interferometer operation near maximal dependence on laboratory rotation. Accordingly, we define the (dimensionless) scale factor for half-revolutions as

$$\Sigma = \max_{\phi_{\rm ref}} \left|\frac{d\langle\hat{\sigma}_{\rm z}\rangle}{d\omega_{\rm S}}\right| \omega. \qquad (2)$$

Rotation sensitivity is given by $S_{\omega_S} = S_\phi\omega/\Sigma$, where S_ϕ is the detection noise of the interferometric phase.

One-dimensional model. First, we consider an idealised situation where the atoms are tightly confined to a ring of radius r, thus restricting the motional degrees of freedom to the azimuthal coordinate θ. Within this ring we assume that two harmonic potentials with trapping frequency ω are displaced by the experimenter in opposite directions at angular speed $\omega_{\rm P}(t)$. In the laboratory frame, both paths end on the opposite side of the ring at $t = T$, imposing the condition $\int_0^T \omega_{\rm P}(t)dt = \pi$. Transforming the Hamiltonian to a state-dependent rotating frame that keeps both potentials stationary leads to

$$\hat{H}_{\uparrow(\downarrow)} = \hat{a}^\dagger\hat{a} + i\frac{R}{\sqrt{2}}\left[\Omega_{\rm S} + \eta_{\uparrow(\downarrow)}\Omega_{\rm P}(\tau)\right](\hat{a} - \hat{a}^\dagger), \qquad (3)$$

where we introduced the function $\eta_{\uparrow(\downarrow)} = +(-)1$, which accounts for the opposite sense of rotation experienced by the two spin states. Furthermore, we defined the dimensionless parameters $\tau = \omega t$, $\Omega_{\rm S} = \omega_{\rm S}/\omega$, $\Omega_{\rm P}(\tau) = \omega_{\rm P}(\tau)/\omega$ and $R = r/x_{\rm ho}$ with $x_{\rm ho} = \sqrt{\hbar/m\omega}$ being the harmonic oscillator length. The Hamiltonians in equation (3) describe forced harmonic oscillators whose unitary time-evolution operators can be expressed in the form of displacement operators $\hat{U}_{\uparrow(\downarrow)} = \exp(\alpha^*_{\uparrow(\downarrow)}\hat{a} - \alpha_{\uparrow(\downarrow)}\hat{a}^\dagger)\exp(i\phi_{\uparrow(\downarrow)})$ via the Magnus expansion [31]. The oscillation amplitudes α are related to physical position and momentum by $\sqrt{2}x_{\rm ho}\alpha = x_{ph} + ip_{ph}/m\omega$. We do not provide here the lengthy explicit expressions of displacement $\alpha_{\uparrow(\downarrow)}$ and phase $\phi_{\uparrow(\downarrow)}$. Substituting the evolution operators into equation (1) yields the population difference after the interference step at time T (see Fig. 1)

$$\langle\hat{\sigma}_{\rm z}\rangle = C_{\rm 1D}\cos\left(\phi_{\rm S} + \phi_{\rm ref}\right), \tag{4}$$

which consists of two factors. The first one is the contrast $C_{\rm 1D} = e^{-|\Delta\alpha|^2/2}$, which depends only on the final relative coherent displacement of the two spin components $\Delta\alpha = \alpha_\uparrow - \alpha_\downarrow = \sqrt{2}r/x_{\rm ho}\int_0^T \omega_{\rm P}(t)e^{-i\omega t}dt$. The second factor is the oscillatory part of the signal which indeed depends on the Sagnac phase $\phi_{\rm S} = 2\pi m r^2\omega_{\rm S}/\hbar$.

This result shows that the Sagnac phase difference accumulated by the atoms remains independent of the temporal profile $\omega_{\rm P}(\tau)$ of the path taken. However, the interferometer contrast, and therefore the signal's sensitivity to rotation is reduced if the final states of the two components are no longer in the ground state of the trap but (symmetrically) displaced. Any choice of temporal path that does not contain Fourier components at the trapping frequency, i.e., for which $\int_0^T \omega_{\rm P}(t)e^{-i\omega t}dt = 0$, will achieve maximum contrast by ensuring that the two wavepackets overlap completely and appear stationary, i.e. $\Delta\alpha = 0$. The maximum speed at which this can be achieved is in principle only limited by the maximum potential energy at which the harmonic oscillator approximation for the confining potentials remains valid.

Two-dimensional model. The one-dimensional model is oversimplified due to the assumption of an infinitely strong radial confinement. In any practical implementation non-negligible radial forces will occur which depend on the rotational speed and which are, in particular, different for the two spin states when $\Omega_{\rm S} \neq 0$. To understand how these inevitable effects impact on the operation of the Sagnac interferometer we consider an exactly solvable two-dimensional model in which atoms are held in the isotropic and harmonic oscillator potential

$$V(x,y) = \frac{1}{2}m\omega^2\left[(x - \cos\hat{\theta}(t))^2 + (y - \sin\hat{\theta}(t))^2\right]. \tag{5}$$

As in the one-dimensional example, both spin components travel in opposite directions. Spin-dependent trap motion is introduced using $\hat{\theta}(t) = \int_0^t du[\omega_{\rm S} + \hat{\sigma}_{\rm z}\omega_{\rm P}(u)]$. A particularly simple analytical description of the system is achieved by introducing the operators $\hat{A}_\pm = \frac{1}{2x_{\rm ho}}(\pm i\hat{x} + \hat{y}) + \frac{x_{\rm ho}}{2}(\pm i\frac{d}{dx} + \frac{d}{dy})$. The Hamiltonian is then given by

$$\hat{H}_{\uparrow(\downarrow)} = \hat{H}_{+,\uparrow(\downarrow)} + \hat{H}_{-,\uparrow(\downarrow)} \tag{6}$$

$$\hat{H}_{\pm,\uparrow(\downarrow)} = [1 \pm \Omega_{\rm S} \pm \eta_{\uparrow(\downarrow)}\Omega_{\rm P}(\tau)]\hat{A}^\dagger_\pm\hat{A}_\pm \mp \hbar R\frac{\hat{A}_\pm - \hat{A}^\dagger_\pm}{2i},$$

where we used the same dimensionless quantities as in equation (3). After transforming into an interaction picture using the transformation $\hat{W} = \hat{W}_+\hat{W}_-$ with $\hat{W}_\pm = e^{\mp\hat{\sigma}_z i\int_0^{\omega T} d\tau\Omega_{\rm P}(\tau)\hat{A}^\dagger_\pm\hat{A}_\pm}$ the problem separates into linearly forced harmonic oscillators. For the elementary sequence of the interferometer protocol we perform a half-rotation of the two traps in opposite directions. As before, this imposes the condition $\theta_{\rm P}(\omega T) = \pi$ on the angular displacement of the potentials in the laboratory frame $\theta_{\rm P}(\tau) = \int_0^\tau d\tau'\Omega_{\rm P}(\tau')$. After the interference step at time T (see Fig. 1) the interferometer signal is given by

$$\langle\hat{\sigma}_{\rm z}\rangle = C_+C_-\cos\left(\phi_+ - \phi_- + \phi_{\rm ref}\right), \tag{7}$$

which depends on the phases

$$\phi_\pm = \frac{R^2}{1\pm\Omega_{\rm S}}\int_0^{\omega T} d\tau\sin[\theta_{\rm P}(\tau)]\sin[(1\pm\Omega_{\rm S})\tau] - \frac{R^2}{4}\int_0^{\omega T}d\tau\int_0^{\omega T}d\tau'\sin\left[\theta_{\rm P}(\tau') + \theta_{\rm P}(\tau) + (1\pm\Omega_{\rm S})(\tau'-\tau)\right]$$
$$- \frac{R^2}{2}\int_0^{\omega T}d\tau\int_0^{\tau}d\tau'\cos\left[(1\pm\Omega_{\rm S})(\tau'-\tau)\right]\sin\left[\theta_{\rm P}(\tau') - \theta_{\rm P}(\tau)\right] \tag{8}$$

and the contrast coefficients

$$C_\pm = \exp\left[-\frac{R^2}{2}\left|\int_0^{\omega T}d\tau\sin[\theta_{\rm P}(\tau)]e^{i(1\pm\Omega_{\rm S})\tau}\right|^2\right]. \tag{9}$$

As an example, we show the scale factor of the two-dimensional interferometer in Fig. 2 for a ring of radius $R = 10$ (measured in terms of harmonic oscillator lengths) and for different values of the rotational speed

Ω_S. The results were obtained for a temporal path of constant speed (flat-top profile), i.e., $\Omega_P(\tau) = \pi/\omega T$ for $0 < \tau < \omega T$. For slow path speeds ($\omega T \gg 1$) the scale factor approaches the adiabatic value $\Sigma_{ad} = \frac{d}{d\Omega_S} 2\pi\Omega_S R^2/(1-\Omega_S^2)^2$. For increasingly faster cycles non-adiabatic effects, i.e., the sloshing motion of the atomic wavepackets in the individual traps due to sudden acceleration, give rise to oscillations in the scale factor. In the extreme case (non-overlapping wavepackets at time T) the scale factor approaches zero. Conversely, times of maximum overlap result in peaked scale factor and are found at the approximate times $\omega T_k = (2k+1)\pi/(1+\Omega_S)$ for integer $k \geq 1$. As shown in the inset of Fig. 2, scale factors at these times are close to or even larger than the adiabatic limit Σ_{ad} for small Ω_S. In principle this permits fast, i.e., non-adiabatic operation of the interferometer.

The data moreover shows that larger Ω_S as well as short operation times can result in better sensitivity, caused by the interplay of three different effects. First, larger centrifugal forces lead to increased effective radius R_{eff} and enclosed interferometer area. While this is the only effect in the adiabatic limit with $R_{eff} = R/(1-\Omega_S^2)$, it leads to non-linearly increasing scale factor beyond the simple Sagnac effect due to the rotation dependent enclosed area. Note, that for $|\Omega_P| + |\Omega_S| > 1$ the centrifugal force overcomes the harmonic confinement and atoms become untrapped. Second, for non-zero Ω_S, the two spin components experience different centrifugal forces and acquire a phase difference from different potential energy in their respective traps, depending on their relative radial motion. Third, the interferometer contrast depends on the laboratory rotation. Overall, the most transparent situation is encountered at $\Omega_S = 0$, where the optimum phase reference angle is $\phi_{ref} = \pm\pi/2$ and the contrast coefficients are equal ($C_+ = C_-$). Here, similar but not identical to the one-dimensional case the contrast is maximised and independent of Ω_S by choosing a path such that $\int_0^{\omega T} d\tau \sin(\theta_P(\tau)) e^{i\tau} = 0$.

Finite temperature. Finally, we consider interferometer operation with thermal states. We can use Glauber-Sudarshan distributions of the density matrix in terms of coherent states $\rho = \int d^2\epsilon p(\epsilon)|\epsilon\rangle\langle\epsilon|$ for each oscillator. For temperatures Θ well above the degeneracy temperature we find the distribution function $p(\epsilon) = \hbar\omega/(\pi k_B\Theta) e^{-\hbar\omega|\epsilon-\alpha_g|^2/k_B\Theta}$ [32]. A technical detail is the appearance of off-sets α_g in the exponent. A state that is prepared in the laboratory frame appears displaced due to our definition of operators in the inertial frame. In the one-dimensional case we have $\alpha_g = iR\Omega_S/\sqrt{2}$, see equation (3). Here, we obtain the thermal signal

$$\begin{aligned}\langle\hat{\sigma}_z\rangle_\Theta &= \int d^2\epsilon p(\epsilon)\langle\epsilon|\hat{U}_\downarrow^\dagger(T)\hat{U}_\uparrow(T)|\epsilon\rangle e^{i\phi_{ref}} + \text{H.c.} \\ &= \langle\hat{\sigma}_z\rangle e^{-\frac{k_B\Theta}{\hbar\omega}|\Delta\alpha|^2} = C_\Theta \cos(\phi_S + \phi_{ref}), \qquad (10)\end{aligned}$$

where $\langle\hat{\sigma}_z\rangle$ is the zero temperature result, see equation (4). The behaviour in the isotropic two-dimensional model is essentially identical but with the contrast dependent on the relative displacement in two dimensions.

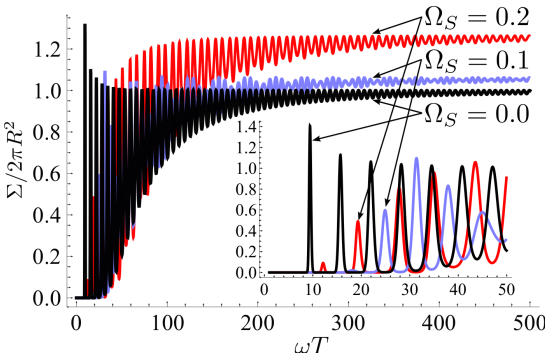

Figure 2. Interferometer scale factor. Results for the two-dimensional case are shown with $R = 10$ and flat-top speed profile $\Omega_P(\tau) = \pi/\omega T$ for $0 < \tau < \omega T$. Plots for $\Omega_S = 0, 0.1, 0.2$ are shown in black, blue and red. The inset shows the same data for $0 < \omega T < 50$.

This shows that finite temperatures result in unchanged interferometer signals, if motional excitation of the traps is avoided or cancelled after trap recombination ($\Delta\alpha = 0$). Otherwise, the zero-temperature reduction in contrast from imperfect state overlap is amplified. This is equivalent to a white light interferometer, where the required precision of wave packet overlap is given by the coherence length. E.g., for the one-dimensional case, a final relative displacement Δx that is purely spatial, i.e., for equal momenta and $\Delta\alpha = \sqrt{m\omega/2\hbar}\langle\Delta\hat{x}\rangle$, the thermal contrast for high temperature can be expressed in terms of thermal wavelength $\lambda_\Theta = h/\sqrt{2\pi m k_B\Theta}$ and harmonic oscillator length x_{ho}

$$C_\Theta = e^{-\left(\frac{1}{2}+\frac{k_B\Theta}{\hbar\omega}\right)|\Delta\alpha|^2} \approx e^{-\frac{\langle\Delta\hat{x}\rangle^2}{2}\left(\frac{1}{2x_{ho}^2}+\frac{\pi}{\lambda_\Theta^2}\right)}. \qquad (11)$$

Experimental implementation with dressed potentials. A scheme for state-dependent circular transport of trappable clock states of ^{87}Rb [29] has been described in [30], using radio-frequency (RF) fields to control atomic motion [33–35]. Interferometry with such RF-dressed potentials has been demonstrated in [36]. The positions of the traps are robustly controlled by the RF phase of a single, linearly polarized field, whose direction defines the recombination points. The small differential Zeeman shift of the clock states, which vanishes for certain parameters [37, 38] leads to nearly identical trapping potentials, thus optimizing state overlap, offering fine control over density dependent effects, and minimizing sensitivity to ambient fields. Recently, a frequency stability of $S_f \approx 4{\cdot}10^{-3}\sqrt{\text{Hz}}$ has been demonstrated with the relevant states in bare potentials [39], limited by inhomogeneous broadening, field fluctuations, and phase noise of the reference clock. The full Ramsey sequence will remove inhomogenous broadening and, in addition, the scheme in [30] enables

simultaneous operation of two closely stacked interferometers, operating in opposite rotational senses. A differential measurement will remove the common fluctuations and phase noise as well as systematic errors from imperfect pulse amplitudes and field aberrations. For uncorrelated particle flux $\dot{n}$ and clock stability S_f, phase detection is limited by $S_\phi^2 = 4\pi^2 S_f^2 T_c^2 D + 1/\dot{n}$, where T_c is the cycle time with duty cycle $D < 1$. For 90% suppression of noise amplitude compared to [39] with $T_c = 1$s and $D = 0.1$, atomic shot noise will be dominant for particle flux up to $10^6 \mathrm{s}^{-1}$. It is within experimental reach to use 1cm diameter loops to achieve corresponding sensitivities on the order of $S_{\omega_S} \approx 10^{-9}\mathrm{rad}/\sqrt{\mathrm{s}}$.

Conclusion & Outlook. An atomic Sagnac interferometer can be implemented with fully confined atoms, at finite temperature, enabling new designs of compact devices. Beyond the principal effects discussed here, actual implementations will need to take into account and optimize effects resulting from inter-atomic collisions, corrugations and noise of trapping potentials, and interplay of thermal motion and finite length spin operations. Optimal control of atomic motion should allow for fast and robust interferometer operation, which reduces phase noise and could in principle achieve sensitivity to rotation beyond the standard Sagnac effect.

We gratefully acknowlegde useful discussions with all members of the MatterWave consortium. This research has been supported by the EU-FET Grant No. 601180 (MatterWave). IL acknowledges funding from the European Research Council under the European Union's Seventh Framework Programme (FP/2007-2013) / ERC Grant Agreement No. 335266 (ESCQUMA).

* thomas.fernholz@nottingham.ac.uk

[1] Schreiber, K. U. & Wells, J.-P. R. Large ring lasers for rotation sensing. *Rev. Sci. Instrum.* **84**, 041101 (2013).

[2] Schreiber, K. U., Klügel, T., Wells, J.-P. R., Hurst, R. B. & Gebauer, A. How to detect the Chandler and the annual wobble of the earth with a large ring laser gyroscope. *Phys. Rev. Lett.* **107**, 173904 (2011).

[3] Clauser, J.F. Ultra-high sensitivity accelerometers and gyroscopes using neutral atom matter-wave interferometry. *Physica B* **151**, 262 (1988).

[4] Barrett, B. et al. The Sagnac effect: 20 years of development in matter-wave interferometry. *Comptes Rendus Physique* **15**, 875 (2014).

[5] Lenef, A. et al. Rotation sensing with an atom interferometer. *Phys. Rev. Lett.* **78**, 760 (1997).

[6] Gustavson, T. L., Bouyer, P., Kasevich, M. A. Precision rotation measurement with an atomic interferometer gyroscope. *Phys. Rev. Lett.* **78**, 2046 (1997).

[7] Cronin, A. D., Schmiedmayer, J. & Pritchard, D. E. Optics and interferometry with atoms and molecules. *Rev. Mod. Phys.* **81**, 1051 (2009).

[8] Gustavson, T. L., Landragin, A. & Kasevich, M. A. Rotation sensing with a dual atom-interferometer Sagnac gyroscope. *Class. Quant. Grav.* **17**, 2385 (2000).

[9] Durfee, D. S., Shaham, Y. K. & Kasevich, M. A. Long-term stability of an area reversible atom-interferometer Sagnac gyroscope. *Phys. Rev. Lett.* **97**, 240801 (2006).

[10] Stockton, J. K., Takase, K. & Kasevich, M. A. Absolute geodetic rotation measurement using atom interferometry. *Phys. Rev. Lett.* **107**, 133001 (2011).

[11] Canuel B. et al. Six-axis inertial sensor using cold-atom interferometry. *Phys. Rev. Lett.* **97**, 010402 (2006).

[12] Dickerson, S. M., Hogan, J. M., Sugarbaker, A., Johnson, D. M. S. & Kasevich, M. A. Multiaxis inertial sensing with long-time point source atom interferometry. *Phys. Rev. Lett.* **111**, 083001 (2013).

[13] Morizot, O., Colombe, Y., Lorent, V., Perrin, H. & Garraway, B. Ring trap for ultracold atoms. *Phys. Rev. A* **74**, 023617 (2006).

[14] Lesanovsky, I. & von Klitzing, W. Time-averaged adiabatic potentials: versatile matter-wave guides and atom traps. *Phys. Rev. Lett.* **99**, 083001 (2007).

[15] Japha, Y., Arzouan, O., Avishai, Y. & Folman, R. Using time-reversal symmetry for sensitive incoherent matter-wave Sagnac interferometry. *Phys. Rev. Lett.* **99**, 060402 (2007).

[16] Baker, P. M. et al. Adjustable microchip ring trap for cold atoms and molecules. *Phys. Rev. A* **80**, 063615 (2009).

[17] Sauer, J. A., Barrett, M. D. & Chapman, M. S. Storage ring for neutral atoms. *Phys. Rev. Lett.* **87**, 270401 (2001).

[18] Jo, G.-B. et al. Long phase coherence time and number squeezing of two Bose-Einstein condensates on an atom chip. *Phys. Rev. Lett.* **98**, 030407 (2007).

[19] Wu, S., Su, E., & Prentiss, M. Demonstration of an area-enclosing guided-atom interferometer for rotation sensing. *Phys. Rev. Lett.* **99**, 173201 (2007).

[20] Ryu, C. et al. Observation of persistend flow of a Bose-Einstein condensate in a toroidal trap. *Phys. Rev. Lett.* **99**, 260401 (2007).

[21] Zawadzki, M. E., Griffin P. F., Riis, E. & Arnold, A. S. Spatial interference from well-separated split condensates. *Phys. Rev. A* **81**, 043608 (2010).

[22] Marti, G. E., Olf, R. & Stamper-Kurn, D. M. Collective excitation interferometry with a toroidal Bose-Einstein condensate. *Phys. Rev. A* **91**, 013602 (2015).

[23] Veretenov, N., Rozhdestvensky, Yu., Rosanov, N. Smirnov, V. & Fedorov, S. Interferometric precision measurements with Bose-Einstein condensate solitons formed by an optical lattice. *Eur. Phys. J. D* **42**, 455 (2007).

[24] McDonald, G. D. et al. Bright solitonic matter-wave interferometer. *Phys. Rev. Lett.* **113**, 013002 (2014).

[25] Helm, J. L., Cornish, S. L. & Gardiner, S. A. Sagnac interferometry using bright matter-wave solitons. *Phys. Rev. Lett.* **114**, 134101 (2015).

[26] Lan, S.-Y. et al. A clock directly linking time to a particle's mass. *Science* **339**, 554 (2013).

[27] Peil, S. & Ekstrom, C. R. Analysis of atom-interferometer clocks. *Phys. Rev. A* **89**, 014101 (2014).

[28] Hafele, J. C. & Keating, R. E. Around-the-world atomic clocks: predicted relativistic time gains. *Science* **177**, 166-168 (1972); ibid. Around-the-world atomic clocks: observed relativistic time gains. pp. 168-170.

[29] Treutlein, P., Hommelhoff, P., Steinmetz, T., Hänsch, T. W. & Reichel, J. Coherence in microchip traps. *Phys. Rev. Lett.* **92**, 203005 (2004).

[30] Fernholz, T., Gerritsma, R. Krüger, P. & Spreeuw, R.

J. C. Dynamically controlled toroidal and ring-shaped magnetic traps. *Phys. Rev. A* **75**, 063406 (2007).

[31] Blanes, S., Casas, F., Oteo, J. A. & Ros, J. The magnus expansion and some of its applications. *Physics Reports* **470(5)**, 151-238 (2009).

[32] Gardiner, C. & Zoller, P. *Quantum Noise: A Handbook of Markovian and Non-Markovian Quantum Stochastic Methods with Applications to Quantum Optics.* (Springer, Berlin 2004).

[33] Lesanovsky, I. et al. Adiabatic radio-frequency potentials for the coherent manipulation of matter waves. *Phys. Rev. A* **73**, 033619 (2006).

[34] Hofferberth, S., Lesanovsky, I., Fischer, B., Verdu, J. & Schmiedmayer,, J. Radiofrequency-dressed-state potentials for neutral atoms. *Nat. Phys.* **2**, 710-716 (2006).

[35] Sherlock, B. E., Gildemeister, M., Owen, E., Nugent, E. & Foot, C. J. Time-averaged adiabatic ring potentials for ultracold atoms. *Phys. Rev. A* **83**, 043408 (2011).

[36] Schumm, T. et al. Matter-wave interferometry in a double well on an atom chip. *Nat. Phys.* **1**, 57 (2005).

[37] Sárkány, P. et al. Controlling the magnetic-field sensitivity of atomic-clock states by microwave dressing. *Phys. Rev. A***90**, 053416 (2014).

[38] Kazakov, G. A. & Schumm, T. Magic radio-frequency dressing for trapped microwave clocks. *Phys. Rev. A* **91**, 023404 (2015).

[39] Szmuk, R., et al. Stability of a trapped-atom clock on a chip. *Phys. Rev. A* **92**, 012106 (2015).